Crystal packing and physical properties of pyridinium tetrabromocuprate(II) complexes assembled *via* hydrogen bonds and aromatic stacking interactions†

Antonio Luque,* Jon Sertucha, Oscar Castillo and Pascual Román

Departamento de Química Inorgánica, Universidad del País Vasco, Apartado 644, E-48080 Bilbao, Spain. E-mail: qipluara@lg.ehu.es

Received (in Montpellier, France) 10th May 2001, Accepted 21st June 2001
First published as an Advance Article on the web 21st August 2001

The compounds $(pyH)_2[CuBr_4]$ (**1**) (pyH = pyridinium) and $(n\text{-MepyH})_2[CuBr_4]$ [*n*-MepyH = *n*-methylpyridinium; $n = 2$ (**2**), 3 (**3**) and 4 (**4**)] have been synthesised from ethanolic solutions containing $CuBr_2$, HBr and the aromatic base in a 1 : 2 : 2 molar ratio. The compounds have been characterised by elemental analysis, IR, UV/VIS and EPR spectroscopies, thermal analysis, variable-temperature magnetic susceptibility measurements and single-crystal X-ray diffraction. In all four crystal structures, the tetrabromocuprate(II) anion is connected to two organic cations through N–H···Br hydrogen bonds to form cation–anion–cation molecular units, which are held together by means of offset face-to-face interactions between the aromatic rings to give one-dimensional chains (**1**, **2** and **4**) or a dimeric entity (**3**). The hydrogen bond and the aromatic stacking interactions are strongly influenced by the position of the methyl group in the pyridinic ring of the cations. The delicate balance between these non-covalent intermolecular forces, together with the electrostatic interactions, ultimately determines the structure and, as a consequence, the physical properties (thermal stability, density and magnetic behaviour) of the compounds. Magnetic susceptibility measurements of powdered samples show that the compounds exhibit weak antiferro- (**1**, **2**, **4**) or ferromagnetic (**3**) magnetic couplings between the copper centres transmitted through the hydrogen bond and the π-stacking interactions. Compound **1** shows a reversible phase transition at 65 °C with a thermal hysteresis of 4 K.

In the last few years, a particular aspect of the field of solid-state chemistry that has received growing attention is the way in which molecules and ions are organised in the solid state to form novel materials with improved electrical, optical, magnetic or catalytic properties.[1] A fundamental requirement for the design of molecules and molecular aggregates having particular desired functions is an understanding of the magnitude and direction of the forces that exist between their constituent units.[2] In this respect, there has been a surge of research activity in the development of specific structural architectures that involve the self-assembly of molecules or ions into well-defined supramolecules *via* intermolecular interactions such as hydrogen bonding and aromatic–aromatic interactions. These non-covalent interactions are some of the most powerful forces to organise structural units in both natural and artificial systems,[3] and they exercise important effects on the organisation and properties of many materials in areas such as biology,[4] crystal engineering[5] and material science.[6] Although the roots of crystal engineering are unquestionably in the organic solid state chemistry field,[7] nowadays, the most tumultuous expansion of the discipline is taking place in the inorganic chemistry area in which systematic studies that investigate the relationships between the characteristics of the individual components (ions or neutral molecules) and the way a crystalline inorganic compound is constructed and organised are being published.[8] These studies are of particular importance not only in the field of coordination solid-state chemistry, in which it is common practice to base the crystallisation of new compounds on empirical rules and local recipes, but also in many areas such as catalysis, bioinorganic and material chemistry, where the coordination complexes play an important role.

In this context, we report herein on the preparation, crystal structure and solid-state properties of four tetrabromocuprate(II) salts using pyridinium (**1**) and *n*-methylpyridinium [$n = 2$ (**2**), 3 (**3**) and 4 (**4**)] as counterions. This work is a part of our studies on hybrid organic/inorganic materials based on copper(II) halides, in which we are attempting to analyse the influence of the organic cation features (size, shape, and nature and position of the substituent) on the packing interactions that govern the crystal organisation and, as a consequence, the properties of this kind of complex.[9–11] The design and synthesis of copper(II) bromides continues to receive much attention owing to their applications in fundamental and applied sciences, ranging from solid-state physics to bioinorganic chemistry. From a physical point of view, copper(II) bromides are excellent candidates for analysing correlations between structural parameters and magnetic properties.[12,13] In the biological field, several studies have shown that tetrahalocuprates(II) of organoammonium cations exhibit potent gastroprotective activity as well as anti-epileptic effects.[14] These pharmacological works have also found that bromo complexes are significantly more active and show a lower cytotoxicity than the analogous chloro complexes. In this context, works analysing the interactions of the tetrabromocuprate(II) anion could be interesting in the understanding of the biological role of these complexes.

Experimental

The starting chemicals were of A. R. grade and used as received. Elemental analyses (C, H, N) were performed on a Perkin–Elmer CHN-240 analyser. Copper analysis was made

† Electronic supplementary information (ESI) available: experimental and calculated X-ray powder diffraction patterns for **1** and TG/DTA thermoanalytical curves for **1**–**4**. See http://www.rsc.org/suppdata/nj/b1/b104085p/

 DOI: 10.1039/b104085p

Table 1 Crystallographic data for compounds **1–4**

	pyH (**1**)	2-MepyH (**2**)	3-MepyH (**3**)	4-MepyH (**4**)
Empirical formula	$C_{10}H_{12}Br_4CuN_2$	$C_{12}H_{16}Br_4CuN_2$	$C_{12}H_{16}Br_4CuN_2$	$C_{12}H_{16}Br_4CuN_2$
M	543.37	571.44	571.44	571.44
Crystal system	Monoclinic	Monoclinic	Monoclinic	Triclinic
Space group	$C2/c$	$C2/c$	$P2_1/n$	$P\bar{1}$
a/Å	8.162(1)	18.789(3)	9.165(1)	8.483(2)
b/Å	14.249(1)	8.744(2)	13.592(2)	9.399(2)
c/Å	13.862(1)	15.518(3)	14.404(3)	13.227(2)
α/°	90.0	90.0	90.0	96.29(3)
β/°	94.77(2)	135.15(3)	102.41(2)	91.29(3)
γ/°	90.0	90.0	90.0	116.41(2)
U/Å^3	1606.6(3)	1798(1)	1752.4(5)	935.9(4)
Z	4	4	4	2
μ/mm^{-1}	11.289	10.093	10.355	9.696
Reflect. measured	2517	2841	5474	5659
Reflect. independent	2342	2591	5097	5438
R_{int}	0.018	0.021	0.042	0.020
Reflect. observed [$I \geqslant 2\sigma(I)$]	1023	1066	1594	1121
R^a	0.043	0.042	0.040	0.045
wR^b	0.050	0.045	0.040	0.045

^{a} $R = \Sigma\|F_o| - |F_c\|/\Sigma|F_o|$. ^{b} $wR = [\Sigma w(|F_o| - |F_c|)^2/\Sigma w|F_o|^2]^{1/2}$.

on a Perkin–Elmer 360 atomic absorption/flame emission spectrometer. The densities were measured by flotation in $CHBr_3$–CCl_4 mixtures.[15] IR spectra (KBr pellets) were recorded on a Perkin–Elmer 4200 spectrometer and UV vis spectra on a Shimadzu 260 spectrometer. Thermoanalytical measurements were made on a Setaram Tag 24 S16 thermobalance (TG/DTA) and a Mettler TA 4000 DSC instrument, using dynamic synthetic air and dry dinitrogen atmospheres (flow rate of 50 cm^3 min^{-1}) and a heating rate of 5 °C min^{-1}. EPR polycrystalline spectra were measured on a Bruker ESP300 spectrometer, operating at the X- (*ca.* 9.5 GHz) and Q-bands (*ca.* 34 GHz). Variable-temperature magnetic susceptibility measurements (2.0–300 K) were performed on a Quantum Design SQUID susceptometer using an applied magnetic field $H = 0.1$ T. Diamagnetic correction terms were estimated from Pascal's constants.[16] X-Ray powder diffraction patterns were recorded on a Philips X'pert powder diffractometer with Cu-Kα radiation ($\lambda = 1.5406$ Å) in steps of 0.02° (2θ) and a fixed-time counting of 4 s.

Syntheses

All manipulations were carried out in an open atmosphere; exposure to air (O_2) is necessary for the synthesis of bromocuprate(II) complexes in HBr media since preparation under anaerobic conditions led to the formation of mixed-valence Cu(II)/Cu(I) compounds.[17,18] Copper(II) bromide (1.00 g, 4.4 mmol), previously dissolved in ethanol, was added dropwise to a stirred ethanolic solution formed by equimolecular amounts of concentrated HBr (1 mL, 8.8 mmol) and the corresponding aromatic amine. After heating for *ca.* 4 h at 60 °C, the resulting black solutions were filtered off and then allowed to stand at room temperature, overnight. The complexes were obtained as black polycrystalline powders that were filtered off, washed with diethyl ether and dried in a dinitrogen stream. For all four compounds, polyhedral dark violet crystals suitable for X-ray crystallographic studies were grown by slow diffusion of n-hexane (20 mL) into an ethanol solution (5 mL) of the complex (0.2 mmol) previously transferred to a 15 mm diameter glass tube. Crystals were filtered off, washed with diethyl ether and dried in a stream of dry dinitrogen. Crystals were essentially opaque due to the absorption of light in the visible region (560 nm) and had a metallic lustre. They were found to be quite stable to light and X-ray exposure, but after three weeks they lost crystallinity and gradually showed a green powder on their surfaces.

$(pyH)_2[CuBr_4]$ (1). Yield 1.05 g, 45% based on copper. Anal. calc. for $C_{10}H_{12}Br_4CuN_2$: C, 22.17; H, 2.22; N, 5.07; Cu, 11.74. found: C, 22.21; H, 2.13; N, 4.98; Cu, 11.62%. IR (ν/cm^{-1}): 3190w, 3135w, 3090w, 3060w, 1630vs, 1595s, 1525vs, 1480vs, 1330s, 1190s, 1050s, 900m, 745s, 675vs and 280w. UV/vis [EtOH–HBr, λ_{max}/nm (ε/M^{-1} cm^{-1})]: 560 (370), 340 (2890), 275 (5600), 235 (2980).

$(2\text{-MepyH})_2[CuBr_4]$ (2). Yield 1.63 g, 65% based on copper. Anal. calc. for $C_{12}H_{16}Br_4CuN_2$: C, 25.22; H, 2.82; N, 4.90; Cu, 11.12; found: C, 25.51; H, 2.77; N, 4.72; Cu, 11.01%. IR (ν/cm^{-1}): 3245m, 3175m, 3120m, 3070m, 2970w, 1625vs, 1610s, 1535s, 1400w, 1280m, 1160m, 1100w, 900m, 750s, 630w, 540w, 505m and 275w. UV/vis [EtOH–HBr, λ_{max}/nm (ε/M^{-1} cm^{-1})]: 560 (300), 340 (1840), 275 (6970), 230 (3150).

$(3\text{-MepyH})_2[CuBr_4]$ (3). Yield 1.46 g, 58% based on copper. Anal. calc. for $C_{12}H_{16}Br_4CuN_2$: C, 25.22; H, 2.82; N, 4.90; Cu, 11.12. found: C, 25.21; H, 2.75; N, 4.85; Cu, 11.00%. IR (ν/cm^{-1}): 3220m, 3190m, 3135m, 3080m, 2920w, 1625m, 1600m, 1540vs, 1500w, 1465s, 1305m, 1240m, 1175w, 890m, 795m, 785m, 675s, 465s and 285w. UV/vis [EtOH–HBr, λ_{max}/nm (ε/M^{-1} cm^{-1})]: 560 (495), 340 (2690), 275 (7980), 240 (2390).

$(4\text{-MepyH})_2[CuBr_4]$ (4). Yield 1.51 g, 60% based on copper. Anal. calc. for $C_{12}H_{16}Br_4CuN_2$: C, 25.22; H, 2.82; N, 4.90; Cu, 11.12; found: C, 25.40; H, 2.83; N, 4.87; Cu, 10.89%. IR (ν/cm^{-1}): 3220m, 3190m, 3135m, 3080m, 2920w, 1634m, 1600s, 1500vs, 1370m, 1310m, 1235m, 1190s, 1110w, 1095w, 790s, 755m, 520w, 450w and 280w. UV/vis [EtOH–HBr, λ_{max}/nm (ε/M^{-1} cm^{-1})]: 560 (280), 345 (1720), 275 (2450), 230 (5240).

X-Ray crystallography

Diffraction intensity data were collected at 295(1) K on an Enraf–Nonius CAD4 diffractometer using graphite-monochromated Mo-Kα radiation ($\lambda = 0.710\,69$ Å) and the conventional ω–2θ scan mode ($\theta_{max} = 30°$). Intensity data were corrected for Lorentz polarisation and absorption[19] effects. Atomic scattering factors and anomalous dispersion terms were taken from ref. 20. The structures were solved by direct methods[21] and refined (on F) by full-matrix least-squares using the X-RAY 76 program package.[22] Anisotropic

thermal parameters were refined for all non-hydrogen atoms. For compound **1**, all hydrogen atoms were clearly visible on a Fourier difference map and isotropically refined. For **2** and **3**, hydrogen atoms were located on a Fourier difference map, but only those attached to nitrogen atoms were isotropically refined; the remaining ones were introduced as fixed contributors in the final structure factor calculations. Crystals of **4** are difficult to grow and small, weakly scattering specimens had to be used, giving a low data to parameter ratio (6 : 1). Thus hydrogen atoms could not be reliably located from difference Fourier maps and they were placed at calculated positions. An empirical weighting scheme[23] was used in the final cycles of refinement to obtain a flat dependence in $\langle \omega \Delta^2 F \rangle$ *vs.* $\langle F_o \rangle$ and $\langle (\sin \theta)/\lambda \rangle$. Final geometrical calculations were carried out with the PARST[24] and PLATON[25] programs. All calculations were performed on a Digital MicroVAX 4500. Crystallographic data and structural refinement parameters are given in Table 1.

CCDC reference numbers 167340–167343. See: http://www.rsc.org/suppdata/nj/b1/b104085p/ for crystallographic data in CIF or other electronic format.

Results and discussion

Description of the crystal structures

The crystal structure of the compounds contain the same basic structural unit, which consists of a discrete $[CuBr_4]^{2-}$ anion (denoted *a*) hydrogen-bonded to two organic cations (denoted *c*), as seen in Fig. 1. The *c*–*a*–*c* molecular units are built through the formation of N–H···Br hydrogen bonds from the pyridinium nitrogen atoms on the bromine atoms in the anions. The molecular units of **1** and **2** have a C_2 symmetry with the copper atom sitting on a crystallographic two-fold axis. Selected bond lengths, bond angles, and hydrogen contacts are listed in Table 2.

As far as the geometry of the $[CuBr_4]^{2-}$ anions is concerned, the Cu–Br bond lengths are in the range 2.34–2.43 Å, being similar to those usually found for analogous compounds.[26–30] The shortest Cu–Br bond lengths are for the bromide ligands not engaged in Cu–Br···H–N hydrogen bonds. The tetrabromocuprate(II) anions in the four compounds present a compressed tetrahedral geometry with two bond angles distinguished from the others (96–104°) by their high values (123–136°). These values show that the geometry is intermediate between square-planar (D_{4h}) and regular tetrahedral (T_d). A quantitative description of the distortion from tetrahedral geometry has been evaluated by the Muetterties and Guggenberger method [$\Delta D = 0$ for a regular tetrahedron and $\Delta D = 100$ for a D_{4h} geometry][31] and the obtained values are listed in Table 2. A semiempirical MO study of the T_d–D_{4h} equilibrium in tetrabromometal complexes[32] indicates that the $[CuBr_4]^{2-}$ anion has a tendency to display the T_d configuration, but it has been pointed out that hydrogen bonding interactions are among the factors that influence the deviation from T_d symmetry in the tetrahalocuprate(II) anions to a near D_{2d} symmetry.[10,29,33] Presumably, this is due to a reduction of the effective charge on the halide ions, thus reducing the electrostatic repulsion between the bromide ions within the $[CuBr_4]^{2-}$ species.

The type and the number of hydrogen bonds around each tetrabromocuprate(II) anion is strongly influenced by the position of the substituent on the pyridinic ring. Two different types of hydrogen bond are found (see end of Table 2). In **1** and **4**, the aromatic cation inherently possesses the ability to approach the anion without steric hindrance and is therefore able to share its N–H proton between two Br acceptors. The N···Br distances are approximately equal, suggesting that the cations have established two nearly symmetric bifurcated hydrogen bonds. In **4**, the Br(4) atom is involved in hydrogen bond interactions with both cations. The two cations around the anion are not coplanar and make dihedral angles of 68 and 84° for **1** and **4**, respectively. In **2** and **3**, the position of the methyl substituent produces steric hindrance with the bromine atoms and the N–H proton only forms a single hydrogen bond with one bromine atom. The two aromatic cations around the tetrabromocuprate(II) anion are coplanar in **3**, whereas they make a dihedral angle of 14.8° in **2**.

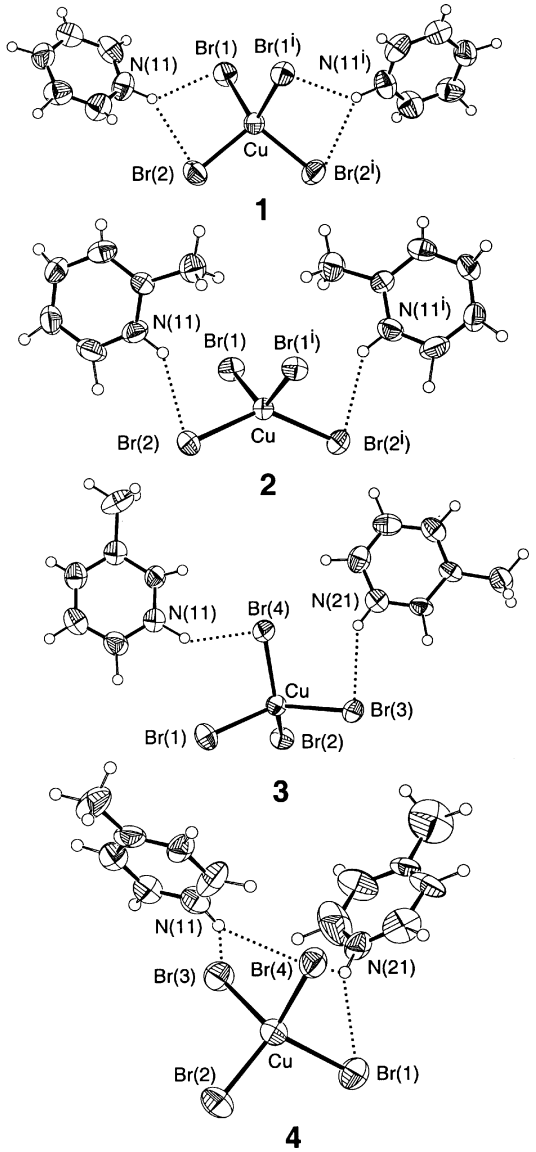

Fig. 1 ORTEP view showing the double N–H···Br hydrogen bonds (dotted lines) between the cations and the $[CuBr_4]^{2-}$ anion in compounds **1**–**4**.

In all four structures the *c*–*a*–*c* molecular entities are held together by means of offset face-to-face aromatic stacking interactions between the rings of adjacent units. The most significant parameters of these interactions are listed in Table 3. The packing patterns of the compounds are quite different. In the crystal structures of **1**, **2** and **4**, anions and cations are packed forming infinite zig-zag one-dimensional chains (Fig. 2) with a *...cac...* sequence and M···M···M angles of 106.1 (**1**), 86.1 (**2**) and 118.0° (**4**) between three successive copper atoms along the chains. The intrachain Cu···Cu distances are >7 Å. It is interesting to note that some subtle differences in the architecture of the chains occur. Whereas the pair of organic cations along the chains of **2** are almost coplanar, in **1** and **4** they are twisted relative to each other, giving bulkier chains. On the other hand, in all the chains the stacked neighbouring cations are offset one from another and show an

Table 2 Selected bond lengths (Å), angles (°), and hydrogen bonds (Å, °) for **1**–**4**[a]

		1	**2**	
	Cu–Br(1)	2.377(1)	2.387(1)	
	Cu–Br(2)	2.364(1)	2.379(3)	
	Br(1)–Cu–Br(1^{i})	100.49(6)	126.41(6)	
	Br(1)–Cu–Br(2)	98.96(4)	100.03(9)	
	Br(1)–Cu–Br(2^{i})	131.28(4)	99.76(4)	
	Br(2)–Cu–Br(1^{i})	131.28(4)	99.76(4)	
	Br(2)–Cu–Br(2^{i})	100.78(6)	135.19(6)	
	Br(1i)–Cu–Br(2^{i})	98.96(4)	100.03(9)	
	ΔD (%)	20.6	20.1	
		3	**4**	
	Cu–Br(1)	2.380(2)	2.419(3)	
	Cu–Br(2)	2.379(1)	2.344(2)	
	Cu–Br(3)	2.389(1)	2.426(2)	
	Cu–Br(4)	2.384(2)	2.394(2)	
	Br(1)–Cu–Br(2)	99.54(5)	104.2(1)	
	Br(1)–Cu–Br(3)	135.74(6)	123.5(1)	
	Br(1)–Cu–Br(4)	97.24(5)	98.4(1)	
	Br(2)–Cu–Br(3)	99.81(6)	101.6(1)	
	Br(2)–Cu–Br(4)	135.16(6)	135.8(1)	
	Br(3)–Cu–Br(4)	96.38(5)	96.6(1)	
	ΔD (%)	25.7	18.8	
	Hydrogen bonds	N···Br	H···Br	<N–H···Br
1	N(11)–H(11)···Br(1)	3.41(1)	2.69(7)	132(6)
	N(11)–H(11)···Br(2)	3.50(1)	2.68(8)	142(6)
2	N(11)–H(11)···Br(2)	3.41(1)	2.60(7)	144(6)
3	N(11)–H(11)···Br(4)	3.27(1)	2.36(8)	144(6)
	N(21)–H(21)···Br(3)	3.36(1)	2.55(7)	146(7)
4	N(11)–H(11)···Br(3^{ii})	3.44(1)	2.57	141
	N(11)–H(11)···Br(4^{ii})	3.39(1)	2.62	131
	N(21)–H(21)···Br(1^{iii})	3.50(1)	2.66	142
	N(21)–H(21)···Br(4^{iii})	3.57(1)	2.83	31

[a] Symmetry codes: (i) $-x+1$, y, $-z+1/2$ for **1**, $-x+1$, y, $-z+3/2$ for **2**; (ii) $x+1$, y, z; (iii) $-x$, $-y$, $-z+1$.

alternating orientation, presumably to minimise electrostatic and steric interactions. The largest offsets (ave. 2.40 Å) are observed for the 4-methylpyridinium salt. The combined effect of a bulky chain and a weak overlap between the cations leads to a less effective packing and the density value of **4** (D_x = 2.028 g cm^{-3}) is smaller than that of **2** (D_x = 2.111 g cm^{-3}). Compound **1** shows the highest density value (D_x = 2.247 g cm^{-3}), owing to the absence of a methyl group in the cation and to a stronger overlap (lateral displacement of 1.80 Å) between the aromatic rings. There are no other important interactions in the crystal structures; the centroid–centroid distance between parallel aromatic cations from two neighbouring chains are longer than 5 Å and the shortest interchain Br···Br contact is 4.36 Å (**1**). Interchain C–H···Br or methyl···methyl contacts have not been observed. So it is quite likely that the interchain interactions are only due to electrostatic effects.

Table 3 Structural parameters of the π-stacking interactions for compounds **1**–**4**[a]

Compound	Interaction[b]	Ring[c]	DC[d]	ANG	DZ	DXY	θ[e]
1	A	1–1^{i}	3.99	0.0	3.59	1.79	26.6
2	A	1–1^{ii}	4.25	0.0	3.66	2.17	30.7
3	A	1–2^{iii}	2.82	2.6	3.46	1.63	25.3
4	A	1–1^{iv}	4.31	0.0	3.59	2.35	33.0
	B	2–2^{v}	4.66	0.0	3.50	2.45	31.7

[a] Symmetry codes: (i) $-x+1/2$, $-y+1/2$, $-z+1$; (ii) $-x+1$, $-y+2$, $-z+1$; (iii) $-x+1$, $-y+1$, $-z$; (iv) $-x+2$, $-y+1$, $-z$; (v) $-x+1$, $-y+1$, $-z+1$. [b] Interaction: see Fig. 2 and 3. [c] Ring: 1 and 2 contain the N(11) and N(21) atoms, respectively. [d] DC: centroid–centroid distance (Å). [e] θ: angle between the DC vector and the normal of the first ring plane.

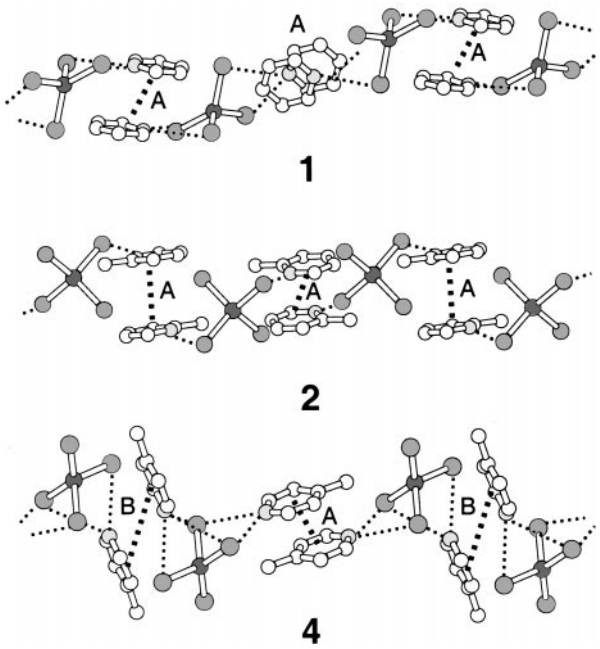

Fig. 2 Fragments of the one-dimensional chains formed by the anions and cations in compounds **1**, **2** and **4**. A and B denote π-stacking interactions (see Table 3). Hydrogen bonds are shown as dotted lines.

In **3**, the *c*–*a*–*c* molecular entity is connected to an inversion-related counterpart through face-to-face interactions involving the two aromatic rings and forming a dimeric group with a Cu···Cu distance of 5.82 Å (Fig. 3). These dimeric entities are essentially isolated in the crystal structure and although the separation between the planes of two aromatic cations from adjacent dimeric units is 3.5 Å, they are so slipped (>3 Å) that no graphite-like interactions may be considered. The shortest interdimer Br···Br distance is 4.45 Å.

We would like to finish this structural description with a brief comment on the common assumption that the tetrabromocuprate(II) salts will be isomorphous to the corresponding chlorides. This frequently is true,[34] but since the overall crystal packing is a consequence of a delicate balance between electrostatic interactions, hydrogen bond and aromatic stacking interactions, it is not surprising to find that isomorphism is not always found. Indeed, compound **4** is not isomorphous with the analogous (4-MepyH)$_2$[CuCl$_4$] salts.[35] As far as we are aware, the crystal structures of the analogous tetrachloro complexes of **1**–**3** have not yet been reported.

EPR spectroscopy and magnetic behaviour

EPR spectra of the compounds were recorded on powdered samples at both the X- (4.2–300 K) and Q-bands (100–300 K). No significant variations have been observed over this range of temperatures. The X-band data are listed in Table 4. X-Band spectra of **1** and **3** show isotropic signals with *g*

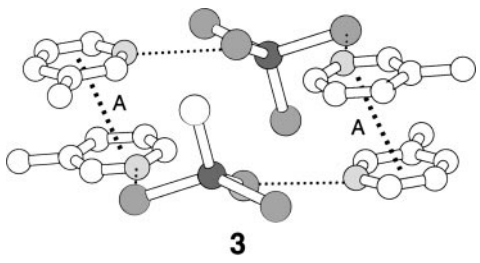

Fig. 3 Ball-and-stick representation showing the dimeric entity in **3**.

Table 4 EPR and magnetic data for **1**–**4**

	1	2	3	4
X-Band EPR data				
$g_{\parallel}$		2.28		2.28
$g_{\perp}$		2.06		2.08
$\langle g \rangle$	2.18	2.13	2.10	2.15
Curie–Weiss fit				
C/cm^3 K mol^{-1}	0.45	0.42	0.40	0.44
Θ/K	−2.71	−1.10	0.92	−0.40
Magnetic model fit				
J/cm^{-1}	−2.20	−0.85	1.03	−0.40
$J\,k^{-1}$/K	−3.17	−1.22	1.48	−0.58
$\lvert D \rvert$/cm^{-1}			0.3	
g	2.16	2.13	2.08	2.17
$R \times 10^5$	1.7	2.3	2.7	1.1

tensor values of 2.18 and 2.10, respectively. The spectra remain essentially unchanged upon cooling the sample from 300 to 30 K, and at lower temperatures the linewidth increases from 800 to 1000 G, being much broader than those for (4-aminopyridinium)$_2$[CuBr$_4$]·H$_2$O.[11] In an attempt to resolve the spectra, Q-band EPR spectroscopy was used. Although the spectra seem to correspond to an axial g tensor, they were not well-resolved due to a rather large linewidth. For **2** and **4**, X- and Q-band axial-type spectra were obtained at all temperatures, which is consistent with the compressed tetrahedral stereochemistry of the chromophore and the relation $g_{\parallel} \gg g_{\perp} > 2.0$ indicates a $d_{x^2-y^2}$ ground state.[29]

The magnetic susceptibility data for the complexes have been measured over the temperature range 2–300 K. The room temperature magnetic moments range from 1.79 to 1.89 μ_B and are typical for one non-interacting d^9 copper(II) ion. The magnetic susceptibility data for all compounds follow a Curie–Weiss law at $T > 40$ K (Table 4). Thermal variations of reciprocal susceptibility and the $\chi_m T$ product of **2** are shown in Fig. 4. The overall appearance of the $\chi_m T$ *vs.* T curves are indicative of weak antiferromagnetic interactions between the Cu(II) centres for **1**, **2** and **4**. The χ_m *vs.* T curve of compound **1** exhibits a maximum at 4 K (Fig. 5).

Considering the structural features of compounds **1**, **2** and **4**, the experimental data were analysed using the Heisenberg model with exchange interaction between pairs of Cu(II) ions with spins S_i and S_j of the form:

$$H = -2\sum_{i>j} J_{ij} S_i S_j \qquad (1)$$

where we assumed interactions between nearest neighbour copper ions in a chain (*i.e.*, $J_{ij} = J$ for $j = i \pm 1$ and $J_{ij} = 0$ otherwise).

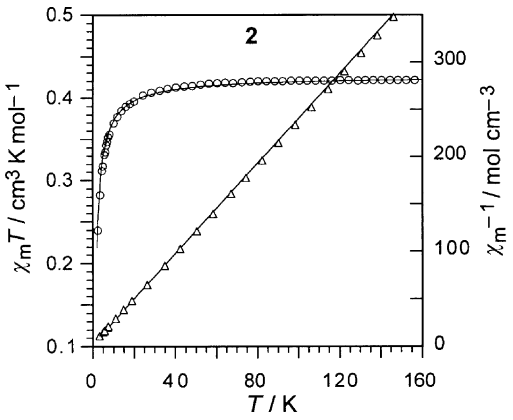

Fig. 4 Thermal variation of the reciprocal magnetic susceptibility and $\chi_m T$ for compound **2**. Solid lines represent the best fit to the theoretical model.

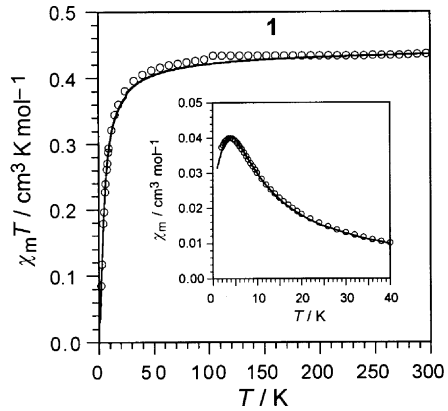

Fig. 5 Thermal dependence of $\chi_m T$ for compound **1**: (○) experimental data; (——) best theoretical fit (see text). The inset shows the region of the susceptibility maximum in the χ_m *vs.* T plot.

In order to evaluate the magnitude of the exchange coupling constant we have used the polynomial expression developed by Hall to describe the results graphically presented by Bonner and Fisher[36] for a uniformly spaced chain of spins with $S = 1/2$:

$$\chi_m = \frac{Ng^2\beta^2}{kT}\left[\frac{A + Bx + Cx^2}{1 + Dx + Ex^2 + Fx^3}\right] \qquad (2)$$

where $x = |J|/kT$, N and k are the Avogadro and Boltzmann constants, β is the Bohr magneton, $A = 0.250$, $B = 0.150$, $C = 0.3009$, $D = 1.9862$, $E = 0.6885$ and $F = 6.0626$. The least-squares best-fit results are listed in Table 4. R is the agreement factor defined as $R = \Sigma_i[(\chi_m)_{obs}(i) - (\chi_m)_{calc}(i)]^2/\Sigma_i[(\chi_m)_{obs}(i)]^2$. The calculated g and J values are in good agreement with those deduced from the ESR spectra and Curie–Weiss fit, respectively. At high temperatures ($|J|/kT \ll 1$) eqn. (2) becomes a Curie–Weiss law with $\Theta = 1.38 \times J/k$, and from the observed Θ values, J/k exchange parameters of −1.96, −0.80 and −0.30 K should be expected, similar to the calculated ones. Therefore, as expected, the 1D Heisenberg model gives a good representation of the magnetic behaviour of these compounds. The overlap between adjacent aromatic rings and the hydrogen bond interactions most likely provide the exchange pathways for the small antiferromagnetic coupling observed. In this respect, weak magnetic couplings across aromatic (pyrazolyl and 2,2′-bipyridine rings) π-stacking interactions were reported[37] and hydrogen bonding has been extensively demonstrated to be a powerful tool for generating magnetic interactions and for propagating them in both inorganic[38] and organic solids.[39]

In the case of **3** the product $\chi_m T$ remains practically constant up to around 50 K, and it increases sharply at lower temperatures to attain a value of 0.48 cm^3 mol^{-1} K at 2 K (Fig. 6). This fact, together with the positive value calculated for Θ, suggests the presence of weak ferromagnetic interactions. The shape of the magnetisation curve at 2.0 K and the value of the saturation are also as expected for the case of ferromagnetic coupling between local spin doublets. The magnetic data were analysed through the Hamiltonian:

$$H = -2JS_1S_2 + S_1DS_2 \qquad (3)$$

where the first term accounts for the isotropic exchange interaction between two spin doublets ($S_1 = S_2 = 1/2$) and the second one concerns the zero-splitting of the triplet state. The best fit results through least-squares analysis[40] are listed in Table 4.

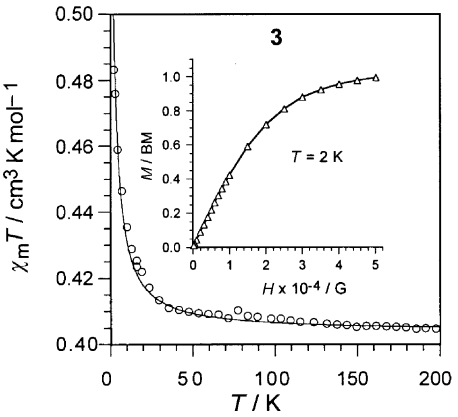

Fig. 6 Thermal dependence of $\chi_m T$ for compound **3**: (○) experimental data; (——) best theoretical fit (see text). The inset shows the field dependence of the magnetisation at 2 K: (△) experimental data; (——) a guide to the eye.

Thermal behaviour

The thermal behaviour of the compounds have been deduced from their TG/DTA curves in both synthetic air and dinitrogen atmospheres (see ESI). An outstanding feature in the thermal degradation of **1** is an endothermic peak at approximately 65 °C, which has been assigned to a phase transition (Fig. 7). TG analysis shows no weight change at this point. The process is reversible, indicating thermal hysteresis. DSC analysis showed a sharp endothermic peak at 67 °C during the heating measurements, as well as an exothermic peak at 63 °C during the cooling measurements. The calculated enthalpies are 5.1 and −4.9 kJ mol^{-1}, respectively. The value of the phase transition enthalpy is comparable to those of analogous tetrabromocuprate(II) complexes and it is lower than those reported for organoammonium tetrachlorocuprate(II) salts.[41]

X-Ray powder diffraction spectra were recorded above and below the transition temperature, with the pattern of both phases being significantly different. Some of the diffraction lines of the room temperature phase diagram are reproduced in the high-temperature one but a shift to lower Bragg angles and changes in the intensities are observed (see ESI). The high-temperature X-ray pattern has been indexed[42] on the basis of the primitive monoclinic cell: $a = 8.779(9)$, $b = 13.884(6)$, $c = 13.440(8)$ Å , $\beta = 92.63(4)°$, $U = 1636(3)$ Å^3 and $D_x = 2.20$ g cm^{-3}. This seems to indicate that there is a change in the internal structure with a slight increase in the volume unit cell.

The X-band EPR spectra show isotropic signals for both low- and high-temperature phases. With increasing temperature, the g tensor value of 2.18 gradually decreases from room temperature to 60 °C and an abrupt drop of the value is observed in the range 60–70 °C to attain a constant value of 2.11 at higher temperatures. This change is accompanied by an increase of the linewidth.

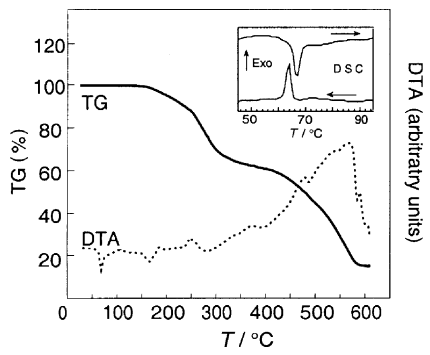

Fig. 7 Thermoanalytical curves (TG and DTA) for compound **1** in air atmosphere. The insert shows the DSC analysis upon heating and cooling.

Structural phase transitions are quite common in copper(II) halide salts and with hydrogen bonding cations they are usually associated with disordering of the cation and a concomitant weakening of N–H···X hydrogen bonds.[43] The weakening of the hydrogen bonds increases the charge density on the halide ions of the $[CuX_4]^{2-}$ anion, which will relax its co-ordination geometry toward tetrahedral in order to minimise the electrostatic repulsion between the halide ions. For several tetrachlorocuprate(II) salts discontinuous thermochromic phase transitions are observed with a green ↔ yellow ↔ orange colour progression as the distortion of the anion with respect to the ideal tetrahedral geometry decreases. The enthalpies of the phase transitions are greater than those observed in the corresponding tetrabromocuprate(II) salts owing to the decreased ionic radii of the chloride ion over that of the bromide ion (1.80 *vs.* 1.95 Å), which usually permits a larger distortion of the tetrachlorocuprate(II) anions from the T_d geometry.[41,43] On the other hand, possible changes of colour are not observed for tetrabromocuprate(II) salts due to the very dark colour of the crystals, attributable to the broad charge transfer bands that spread over the whole visible range.

No phase transitions were observed in the thermal evolution of compounds **2**–**4** from room temperature to their melting points at 115 (**2**), 135 (**3**) and 110 °C (**4**). The melting enthalpies are 40 (**2**), 45 (**3**) and 30 kJ mol^{-1} (**4**). The melting points, the enthalpies and the density values are in the order **3** > **2** > **4**. The phase transition of **1** and the melting processes do not show significant dependence on the nature of the environmental gas, but the decomposition pathway of the liquid and the final residues are affected by the surrounding atmosphere. Under air atmosphere, the compounds decompose endothermically at 140 (**2**), 160 (**3**) and 175 °C (**4**) with the oxidation of the organic units to give copper(II) bromide followed by a strong exothermic loss of bromine to give copper(II) oxide as the final product above 610 °C. No other peak belonging to Cu or another copper oxide were found in the X-ray powder diffractogram of the final stable residue. In a nitrogen atmosphere, all degradation processes are endothermic and they lead, without intermediate stable species, to powdered metallic copper as the final product above 700 °C. No peaks corresponding to $CuBr_2$ or CuBr could be identified. These results suggest that organic cation pyrolysis under an inert atmosphere can produce, directly or indirectly, the reduction of Cu(II) to Cu(0). Some authors have suggested that the thermal degradation of organoammonium halometalate complexes in inert atmospheres is an excellent method of obtaining powdered metals of great reactivity.[44]

Conclusions

The crystal architecture of the copper(II) bromide and *n*-methylpyridine system ($n = 0, 2, 3, 4$) proves to be very rich. A major component in this richness is the ability of the pyridinium cations to partake in aromatic π-stacking interactions and to form different types of hydrogen bonds between the >N–H$^+$ groups and the Br atoms of the tetrabromocuprate(II) anions. These non-covalent interactions, together with the electrostatic forces, induce a compactness in the crystalline lattices and provide magnetic exchange pathways in these hybrid organic/inorganic materials, which behave as low-dimensional magnetic materials.

Acknowledgements

We are grateful for financial support from the Universidad del País Vasco/Euskal Herriko Unibertsitatea (UPV/EHU)

(Project 169.310-EA857/2000). J. S. thanks the Spanish Government for a doctoral fellowship (grant no. AP94.42172547).

References

1 (*a*) J.-M. Lehn, *Supramolecular Chemistry: Concepts and Perspectives*, VCH, Weinheim, 1995; (*b*) *Perspectives in Supramolecular Chemistry*, ed. G. R. Desiraju, Wiley, Chichester, 1996, vol. II; (*c*) *Crystal Enginering: from Molecules and Crystals to Materials*, ed. D. Braga, F. Grepioni and A. G. Orpen, Kluwer Academic Publishers, Dordrecht, 1999.

2 C. B. Aakeröy and K. R. Seddon, *Chem. Soc. Rev.*, 1993, **22**, 397.

3 (*a*) L. J. Barbour, L. R. MacGillivray and J. L. Atwood, *Supramol. Chem.*, 1996, **7**, 167; (*b*) K. M. Guckian, B. A. Schweitzer, R. X. F. Ren, C. J. Sheils, D. C. Tahmassebi and E. T. Kool, *J. Am. Chem. Soc.*, 2000, **122**, 2213; (*c*) C. Janiak, *J. Chem. Soc., Dalton Trans.*, 2000, 3885; (*d*) K. Müller-Dethlefs and P. Hobza, *Chem. Rev.*, 2000, **100**, 143; (*e*) A. Angeloni and A. G. Orpen, *Chem. Commun.*, 2001, 343.

4 (*a*) C. A. Hunter, *Chem. Soc. Rev.*, 1994, 102; (*b*) G. R. Desiraju and T. Steiner, *The Weak Hydrogen Bond in Structural Chemistry and Biology*, Oxford University Press, Oxford, 1999.

5 (*a*) F. H. Allen, V. J. Hoy, J. A. K. Howard, V. R. Thalladi, G. R. Desiraju, C. C. Wilson and G. J. McIntyre, *J. Am. Chem. Soc.*, 1997, **119**, 3477; (*b*) G. Aullon, D. Bellamy, A. G. Orpen, L. Brammer and E. A. Bruton, *Chem. Commun.*, 1998, 653; (*c*) G. R. Lewis and A. G. Orpen, *Chem. Commun.*, 1998, 1873; (*d*) A. L. Gillon, A. G. Orpen, J. Starbuck, X. M. Wang, Y. Rodríguez-Martín and C. Ruiz-Pérez, *Chem. Commun.*, 1999, 2287; (*e*) L. Brammer, J. C. Mareque Rivas, R. Atencio, S. Fang and F. C. Pigge, *J. Chem. Soc., Dalton Trans.*, 2000, 3855; (*f*) B. Dolling, A. L. Gillon and A. G. Orpen, *Chem. Commun.*, 2001, 567.

6 (*a*) M. C. Etter, *J. Am. Chem. Soc.*, 1987, **109**, 7786; (*b*) J. M. A. Robinson, D. Philp, K. D. M. Harris and B. M. Kariuki, *New J. Chem.*, 2000, **24**, 799.

7 (*a*) G. M. J. Schmidt, *Pure Appl. Chem.*, 1971, **27**, 647; (*b*) G. R. Desiraju, *Crystal Engineering: The Design of Organic Solids*, Elsevier, Amsterdam, 1989; (*c*) C. A. Hunter, *Angew. Chem., Int. Ed. Engl.*, 1993, **32**, 1584; (*d*) R.-F. Liao, J. W. Lauher and F. W. Fowler, *Tetrahedron*, 1996, **9**, 3153; (*e*) A. L. Gillon, G. R. Lewis, A. G. Orpen, S. Rotter, J. Starbuck, X. M. Wang, Y. Rodríguez-Martín and C. Ruiz-Pérez, *J. Chem. Soc., Dalton Trans.*, 2000, 3897.

8 (*a*) D. Braga, F. Grepioni and E. Parisini, *J. Chem. Soc., Dalton Trans.*, 1995, 287; (*b*) S. B. Copp, K. T. Holman, J. O. S. Sangster, S. Subramanian and M. J. Zaworotko, *J. Chem. Soc., Dalton Trans.*, 1995, 2233; (*c*) P. Day, *J. Chem. Soc., Dalton Trans.*, 1996, 701; (*d*) D. Braga, *J. Chem. Soc., Dalton Trans.*, 2000, 3705; (*e*) S. C. James, Y. G. Lawson, N. C. Norman and M. J. Qualy, *Acta Crystallogr., Sect. C*, 2000, **56**, 427; (*f*) A. G. Orpen and M. J. Quayle, *J. Chem. Soc., Dalton Trans.*, 2001, 1601.

9 P. Román, J. Sertucha, A. Luque, L. Lezama and T. Rojo, *Polyhedron*, 1996, **15**, 1253.

10 A. Luque, J. Sertucha, L. Lezama, T. Rojo and P. Román, *J. Chem. Soc., Dalton Trans.*, 1997, 847.

11 J. Sertucha, A. Luque, F. Lloret and P. Román, *Polyhedron*, 1998, **17**, 3875.

12 (*a*) C. P. Landee, M. M. Turnbull, C. Galeriu, J. Giantsidis and F. M. Woodward, *Phys. Rev. B*, 2001, **63**, 100402; (*b*) T. Matsumoto, Y. Miyazaki, S. A. Albrecht, C. P. Landee, M. M. Turnbull and M. Sorai, *J. Phys. Chem. B*, 2000, **104**, 9993.

13 R. D. Willett, *Coord. Chem. Rev.*, 1991, **109**, 181.

14 (*a*) D. G. Craciunescu, M. T. Gutiérrez-Ríos, E. Parrondo-Iglesias, C. Molina, A. Doadrio-López, E. Gastón de Iriarte and C. Guirvu, *An. R. Acad. Farm.*, 1989, **55**, 329; (*b*) D. Frechilla, B. Lasheras, M. Ucelay, E. Parrondo, G. Craciunescu and E. Cenarruzabeitia, *Arzneim.-Forsch.*, 1991, **41**, 247.

15 P. Román and J. M. Gutiérrez–Zorrilla, *J. Chem. Educ.*, 1985, **62**, 167.

16 A. Earnshaw, *Introduction to Magnetochemistry*, Academic Press, London, New York, 1968.

17 A. Bencini and F. Mani, *Inorg. Chim. Acta*, 1984, **87**, L9.

18 R. D. Willett and K. Halvorson, *Acta Crystallogr., Sect. A*, 1988, **44**, 2068.

19 N. Walker and D. Stuart, *Acta Crystallogr., Sect. A*, 1983, **39**, 158.

20 *International Tables for X-Ray Crystallography*, Kynoch Press, Birmingham, 1974, vol. IV.

21 P. T. Beurskens, G. Admiraal, G. Beurskens, W. P. Bosman, S. García-Granda, R. O. Gould, J. M. M. Smith and C. Smykalla, The DIRDIF program system, Technical Report of the Crystallography Laboratory, University of Nijmegen, The Netherlands, 1992.

22 J. M. Stewart, P. A. Machin, C. W. Dickinson, H. L. Ammon, H. Heck and H. Flack, The X-RAY 76 System, Technical report TR-446, Computer Science Center, University of Maryland, College Park, MD, USA, 1976.

23 M. Martínez-Ripoll and F. H. Cano, Programa PESOS, Instituto Rocasolano, CSIC, Madrid, 1975.

24 M. Nardelli, *Comput. Chem.*, 1983, **7**, 95.

25 A. L. Spek, *Acta Crystallogr., Sect. A*, 1990, **46**, C34.

26 B. J. Hathaway, *Struct. Bonding*, 1984, **57**, 55.

27 (*a*) H. Place and R. D. Willett, *Acta Crystallogr., Sect. C*, 1988, **44**, 34; (*b*) T. Manfredini, G. C. Pellacani, A. Bonamartini-Corradi, L. P. Battaglia, G. G. T. Guarini, J. G. Giusti, G. Pon, R. D. Willett and D. X. West, *Inorg. Chem.*, 1990, **29**, 2221.

28 (*a*) T. J. Coffey, C. P. Landee, W. T. Robinson, M. M. Turnbull, M. Winn and F. M. Woodward, *Inorg. Chim. Acta*, 2000, **303**, 54; (*b*) G. Pon, R. D. Willett, B. A. Prince, W. T. Robinson and M. N. Turnbull, *Inorg. Chim. Acta*, 1997, **255**, 325.

29 M. R. Sunberg, R. Kivekäs, J. Ruiz, J. M. Moreno and E. Colacio, *Inorg. Chem.*, 1992, **31**, 1062.

30 (*a*) H. Place and R. D. Willett, *Acta Crystallogr., Sect. C*, 1987, **43**, 1497; (*b*) T. E. Grigereit, B. L. Ramakrishna, H. Place, R. D. Willett, G. C. Pellacani, T. Manfredini, L. Menabue, A. Bonamartini and L. Battaglia, *Inorg. Chem.*, 1987, **26**, 2235.

31 E. L. Muetterties and L. J. Guggenberger, *J. Am. Chem. Soc.*, 1974, **96**, 1748.

32 P. Pelikán and M. Liska, *Collect. Czech. Chem. Commun.*, 1984, **49**, 2837.

33 D. Reinen, M. Atanasov, G. S. Nicolov and F. Steffens, *Inorg. Chem.*, 1988, **27**, 1678.

34 (*a*) H. Place and R. D. Willett, *Acta Crystallogr., Sect. C*, 1987, **43**, 1050; (*b*) R. D. Willett, H. Place and M. Middleton, *J. Am. Chem. Soc.*, 1988, **11**, 8639.

35 P. Román, A. Luque and J. A. Pozo, *Mater. Res. Bull.*, 1992, **27**, 989.

36 (*a*) J. W. Hall, Ph. D. Thesis, University of North Carolina, 1977; (*b*) J. C. Bonner and M. E. Fisher, *Phys. Rev. A*, 1964, **135**, 640.

37 (*a*) A. J. Amoroso, J. C. Jeffery, P. L. Jones, J. A. McCleverty, P. Thornton and M. D. Ward, *Angew. Chem., Int. Ed. Engl.*, 1995, **34**, 1443; (*b*) M. C. Muñoz, M. Julve, F. Lloret, J. Faus and M. Andruh, *J. Chem. Soc., Dalton Trans.*, 1998, 3125.

38 (*a*) E. Escriva, J. Server-Carrio, J. García-Lozano, F. V. Folgado, F. Sapina and L. Lezama, *Inorg. Chim. Acta*, 1998, **279**, 58; (*b*) Y. Yamada, N. Ueyama, T. Okamura, W. Mori and A. Nakamura, *Inorg. Chim. Acta*, 1998, **276**, 43.

39 N. Daro, J. P. Sutter, M. Pink and O. Khan, *J. Chem. Soc., Perkin Trans. 2*, 2000, 1087.

40 O. Khan, *Molecular Magnetism*, VCH, New York, 1993.

41 A. Uehara, A. Iimura, K. Shimizu, S. Morita, A. Yoshifuji and R. Tsuchiya, *Thermochim. Acta*, 1984, **77**, 299.

42 J. Rodriguez-Carvajal, FULLPROF Program for Rietveld Pattern Matching Analysis of Powder Diffraction Patterns, Grenoble, 1997.

43 (*a*) D. R. Bloomquist and R. D. Willett, *Coord. Chem. Rev.*, 1982, **47**, 125; (*b*) D. R. Bloomquist, M. R. Pressprich and R. D. Willett, *J. Am. Chem. Soc.*, 1988, **110**, 739; (*c*) S. Haddad and R. D. Willett, *Inorg. Chem.*, 2001, **40**, 2457.

44 J. R. Allan, *Thermochim. Acta*, 1992, **200**, 355.